ELSEVIER

Journal of Structural Geology 28 (2006) 1623–1639

JOURNAL OF STRUCTURAL GEOLOGY

www.elsevier.com/locate/jsg

Structural record of the mechanical evolution of mixed zones in faulted poorly lithified sediments, Rio Grande rift, New Mexico, USA

Geoffrey C. Rawling [a,*], Laurel B. Goodwin [b]

[a] *New Mexico Bureau of Geology and Mineral Resources, 2808 Central Avenue SE, Albuquerque, NM 87106-2245, USA*
[b] *Department of Geology and Geophysics, University of Wisconsin—Madison, 1215 West Dayton Street, Madison, WI 53706-1692, USA*

Received 20 December 2005; received in revised form 2 June 2006; accepted 21 June 2006
Available online 8 August 2006

Abstract

Structural characteristics of faults in poorly lithified sediments of the Albuquerque Basin, New Mexico, USA record the structural and mechanical development of mixed zones. Mixed zones exhibit macroscopically ductile structures, including foliations and lineations, formed by sediment disaggregation and penetrative particulate flow accompanied to varying degrees by cataclasis in sandy sediments. These structures are overprinted by deformation bands, indicating a temporal and mechanical shift to localized cataclasis. The observations are consistent with the inferred consolidation history (progressive overconsolidation) of the fault and host sediments, including tectonic compaction in the fault zone, as well as predictions from critical state soil mechanics theory. These results have implications for the interpretation of fault-zone deformational histories in general. Structures formed before complete lithification are likely to be preserved even where overprinted by later structures, as deformation is likely to become increasingly localized with lithification. Mixed zones may also complement fault cores and contribute to the sealing capacity of faults, as the processes by which they are produced demonstrably reduce permeability. A better understanding of how they form therefore contributes to understanding the mechanics of fault seal development in poorly lithified materials, which are physically distinct from fully lithified rock.

Keywords: Fault zone; Sediment; Critical state soil mechanics; Fluid flow

1. Introduction

Following the recognition of the impact of faults on subsurface fluid flow (Smith et al., 1990; Bredehoeft et al., 1992; Knipe, 1993; Haneberg, 1995), much work has focused on characterizing the internal structure and hydrologic properties of fault zones (Lindsay et al., 1993; Antonellini and Aydin, 1994; Antonellini et al., 1994; Caine et al., 1996; Evans et al., 1997; Lehner and Pilaar, 1997; Heynekamp et al., 1999; Sigda et al., 1999; Rawling et al., 2001; Aydin and Eyal, 2002; Doughty, 2003; Bense et al., 2003). Field studies of fault zones in crystalline and lithified, low porosity sedimentary rocks deformed in the seismogenic zone have resulted in a widely accepted conceptual fault zone model (Chester and Logan, 1986; Chester et al., 1993; Caine et al., 1996). The basic structural unit of faults in these rocks is the fracture, whereas in high-porosity sedimentary rocks it is the deformation band (e.g., Aydin and Johnson, 1978). In both cases, the fault zone includes two architectural elements bounded by protolith with no fault-related deformation structures: A core zone of gouge or cataclasite, which is the locus of most of the deformation, flanked by damage zones with abundant fractures or deformation bands.

This conceptual model is not, however, entirely appropriate for faults in poorly lithified sediments, which have elastic properties transitional between those of soil (i.e., completely unlithified sediment) and rock. Haneberg (1999) calculated values of Young's modulus for Santa Fe Group sediments, which are the focus of this study, using P-wave velocity

* Corresponding author. Tel.: +1 505 366 2535; fax: +1 505 835 6333.
E-mail addresses: geoff@gis.nmt.edu (G.C. Rawling), laurel@geology.wisc.edu (L.B. Goodwin).

0191-8141/$ - see front matter © 2006 Elsevier Ltd. All rights reserved.
doi:10.1016/j.jsg.2006.06.008

logs. The resulting dynamic moduli typically have higher values than those determined in static tests (Cheng and Johnston, 1981), and vary from 5 to 20 GPa. Assuming a Poisson's ratio of 0.25, this yields shear moduli from 2 to 8 GPa. These values are greater than those of soils and overlap the low end of the range commonly encountered in lithified sedimentary rocks (cf. Wibberly et al., 1999).

Studies of faults that cut Santa Fe Group sediments which fill the Rio Grande rift, New Mexico, USA have identified a third, physically discrete architectural element, referred to as a mixed zone, which may develop between the core and damage zones where displacement is greater than local average bed thickness (Mozley and Goodwin, 1995; Heynekamp et al., 1999; Sigda et al., 1999; Rawling et al., 2001; Caine et al., 2002). Mixed zones exhibit compositional variability, but are commonly sand and/or gravel-rich, and are typified by heterogeneous deformation, from intact but rotated and attenuated bedding to intermixing of such disparate sediment types as clay and gravel by particulate flow and cataclasis. Mixed zones are structurally, lithologically, and hydrologically distinct from adjacent core and damage zones (Heynekamp et al., 1999; Rawling et al., 2001; Rawling and Goodwin, 2003; J.S. Caine, personal communication, 2003); thus, they are not represented by the simple core zone/damage zone model. The boundaries between mixed and core zones are discrete and sharp, rather than gradational—mixed zones are not simply part of the fault core. In general, they exhibit macroscopically ductile deformation, in the sense of distributed deformation without extensive localization (Rutter, 1986).

The studies mentioned above have addressed fault-zone architecture and cementation patterns, permeability structure, impact on fluid flow, and deformation mechanisms in poorly lithified sediments. Other structural studies of faulted sediments have addressed clay and shale smear processes and clay-rich fault core formation (Lindsay et al., 1993; Lehner and Pilaar, 1997; Doughty, 2003) and displacement/fault length relationships (Wibberly et al., 1999). In this paper, we elucidate the structural and mechanical evolution of faults in poorly lithified sediments, with emphasis on mixed zones—features of these faults that we have shown to be hydrologically significant (Rawling et al., 2001), but which have not received the level of attention that fault cores have enjoyed. We present new outcrop and microstructural data demonstrating that mixed zones record initial, relatively distributed, deformation by sediment disaggregation and particulate flow, followed by cataclasis localized within deformation bands. The nature of cataclasis in sediments deformed at low confining pressure was addressed in an earlier paper (Rawling and Goodwin, 2003).

Faults such as we describe here impact geologic processes of practical significance, such as fault seal. Mixed zones have reduced permeability compared to host sediments, and locally may have permeability equivalent to clay-rich fault cores (Sigda et al., 1999; Rawling et al., 2001). Accurate characterization of faults in poorly lithified sediments is significant because the presence of mixed zones can help maintain the continuity of low permeability fault rock where gaps are present in the clay-rich fault core. A fault seal partly composed of mixed zones may not seal over geologic time, but could compartmentalize hydrocarbon reservoirs and aquifers or significantly affect the tortuosity of flow paths. This may impact hydrocarbon reservoir management and well yields on production timescales, travel times of contaminants in aquifers, and spatial variability of drawdown in water supply wells. The results we present here represent an important first step toward identifying the fundamental mechanical processes that produce fault seal in poorly lithified sediments.

Understanding fault-zone deformation of poorly lithified sediments is also important for reconstructing geologic histories because the resulting structures provide a record of the state of lithification at the time of deformation. Critical state soil mechanics theory predicts that particulate flow deformation mechanisms should be important during faulting of granular materials such as unlithified and poorly lithified sediments (Jones and Addis, 1986). The styles of deformation and overprinting relationships we observe are consistent with predictions from this theory, given the poorly lithified nature of the sediments and their burial history.

2. Study areas

The two faults we studied cut poorly lithified sediments of the Tertiary Santa Fe Group which, except in uncommon areas of calcite cementation, are friable and easily disaggregated with hand tools. The first is a fault located near the center of the Albuquerque Basin, across which Sigda et al. (1999) documented variations in permeability. It appears to be a southern extension of, or splay from, the Santa Ana fault (Sigda et al., 1999; S. Connell, written communication, 2001), which is a major intrabasinal, down-to-the-east, normal fault that is well exposed at the northern margin of the basin (Pazzaglia et al., 1999). The exposures examined here are in the wall of an incised drainage in the city of Rio Rancho, NW of Albuquerque (Fig. 1). Sigda et al. (1999) estimated approximately 10 m of throw on the fault, which cuts sediments of the upper Santa Fe Group. It includes nascent but readily identifiable damage, mixed, and core zones.

The second fault studied is the Sand Hill fault, a major normal fault marking the western margin of the Albuquerque Basin of the Rio Grande rift (Hawley et al., 1995; Fig. 1). It is a growth fault juxtaposing synrift sediments of the Pliocene-Pleistocene upper Santa Fe Group against middle Miocene to Oligocene sediments of the lower and middle Santa Fe Group, with displacement increasing from $\sim$10 to $\sim$600 m down-dip (Connell et al., 1999; Heynekamp et al., 1999; Tedford and Barghoorn, 1999). Stratigraphic constraints suggest that current exposures of the Sand Hill fault were never buried more than 1 km (Connell et al., 1999; Tedford and Barghoorn, 1999, S. Connell, written communication, 2001), corresponding to a maximum overburden pressure of 20–30 MPa. Local preservation of colluvium in the hanging wall provides a record of episodic surface rupture and development of a fault scarp, indicating at least some fault-zone deformation occurred at seismic strain rates. The two study outcrops are portions of those mapped at a scale of 1:100 by Heynekamp et al.

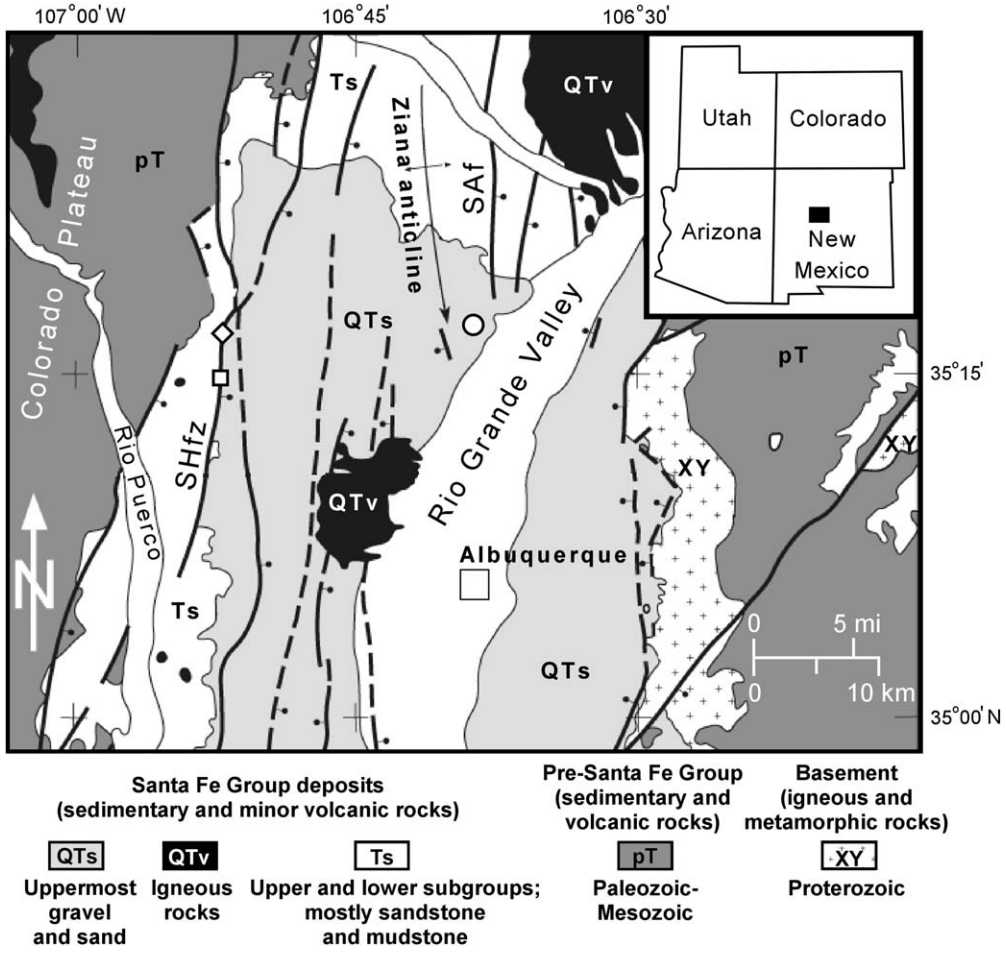

Fig. 1. Study sites in Albuquerque Basin of Rio Grande rift. Inset shows regional location. Sand Hill fault zone (SHfz) sites are Shooting Gallery (square) and Waterfall (diamond). Santa Ana fault (SAf) site is circle. Faults are generalized; not all faults are shown; ball and bar on downthrown side. Modified from Hawley et al. (1995) and Hawley and Whitworth (1996) by S. Connell.

(1999). The outcrops are at approximately the same structural and stratigraphic level, and the fault throw at these exposures is approximately 200 m (Tedford and Barghoorn, 1999). This large-displacement fault exhibits great structural complexity and extensive development of damage, mixed, and core zones.

The syn-rift Santa Fe Group includes dune, fluvial, and playa deposits ranging from clay to gravel. As is typical of continental rift sediments, these are both laterally and vertically discontinuous. Sands are typically immature; lithic arkoses, for example, are common adjacent to the Sand Hill fault (Beckner and Mozley, 1998). Because of this variability, we focus in the following sections on outcrop-specific lithologic variations, which are discussed in the text and associated figures.

3. Macroscopic fault zone structures

3.1. Santa Ana fault

Fig. 2 is a photo and outcrop map of the relatively small displacement Santa Ana fault. Damage zone development is minimal. The mixed zones are composed of a tan, medium-grained sand and a reddish, clay-rich sand, and encompass most of the variation in fault zone thickness. The mixed zones are internally deformed, with a fault-parallel foliation defined by compositional layering (described by variations in mineralogy, grain size, and sorting) and grain-shape preferred orientation locally overprinted with individual deformation bands in a Riedel (R_1) orientation (Fig. 3a, cf. Logan et al., 1992). This is a pattern observed within the mixed zones at all of the outcrops in this study; deformation bands, either singly or clustered, may crosscut each other, but they always overprint a macroscopically ductile foliation. The boundaries between the footwall and hanging wall mixed zones and their respective damage zones are shear zones of coalesced deformation bands (hereafter referred to as deformation band shear zones) (Fig. 3b). The mixed zone contacts and contacts with the clay core are commonly slightly stepped, due to offset along the R_1 deformation bands which terminate at the contact (Fig. 3a). The clay core bounds an elongate and tapered pod of deformed sand similar to the adjacent mixed zone sands.

3.2. Sand Hill fault

3.2.1. Fault zone architecture and planar structures

Fig. 4 shows the internal architecture of the Sand Hill Fault in a schematic cross-section and orientation data for

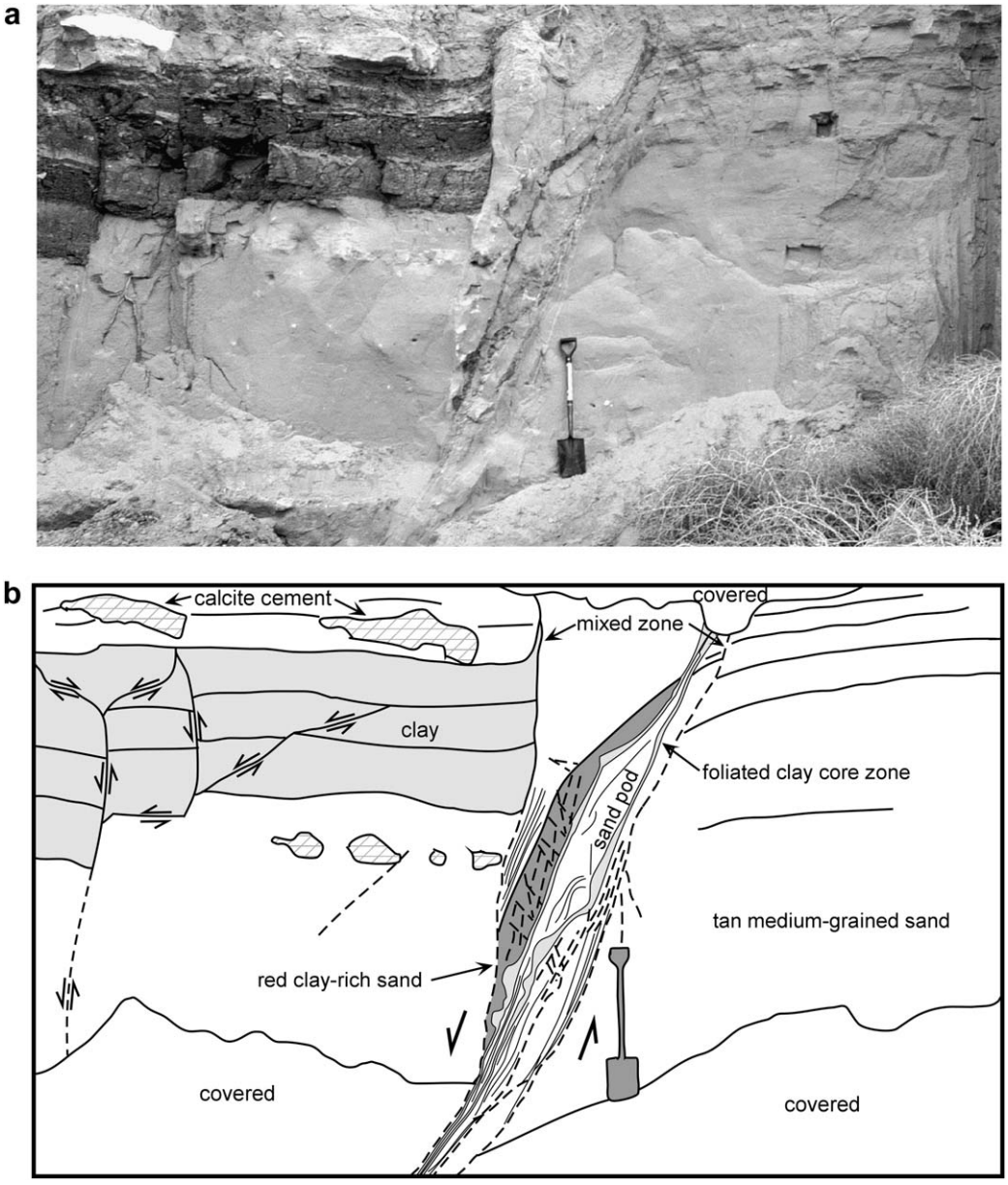

Fig. 2. (a) Photograph and (b) sketch from photograph of Santa Ana fault outcrop. Thick lines are bedding and fault contacts, thin lines are foliations, dashed lines are deformation bands. Shovel is 1 m high. Note that the minor fault in the hanging wall changes dip and forms splays upon entering the clay layers. View is to the southeast.

deformation bands and minor faults within the footwall damage and mixed zones. Extensive calcite cementation is confined to coarse-grained portions of the hanging wall mixed zone; elsewhere diagenetic alteration is limited to clay coatings on sand grains, local growth of euhedral zeolites in pores (Heynekamp et al., 1999), and rare, poorly developed calcite cement. Where not cemented, hanging wall exposures are poor; therefore most of our observations and measurements are from the footwall.

Most deformation bands strike subparallel to the local trace of the fault. Steeply dipping normal-slip deformation bands correspond in orientation and slip sense to R_1 or Y shears (Fig. 4b and f). Reverse-slip deformation bands correspond in orientation to R_2 shears (Fig. 4c and f). Deformation bands of unknown slip sense are both steeply E–NE and W–SW dipping (Fig. 4d). Collectively, the deformation bands accommodate thinning perpendicular to the fault and down-dip extension (Fig. 4a), similar to fractures and small faults observed by Weber et al. (1978) and Aydin and Eyal (2002).

3.2.2. Mesoscopic structures visible in cross section

We excavated several cross-sectional benches through the Sand Hill fault zone and mapped subvertical faces in detail at a scale of 1:10. The sites studied are notable for the lack of discrete, open fractures in both non-cemented and less common cemented areas. The clay contents of faulted sediments

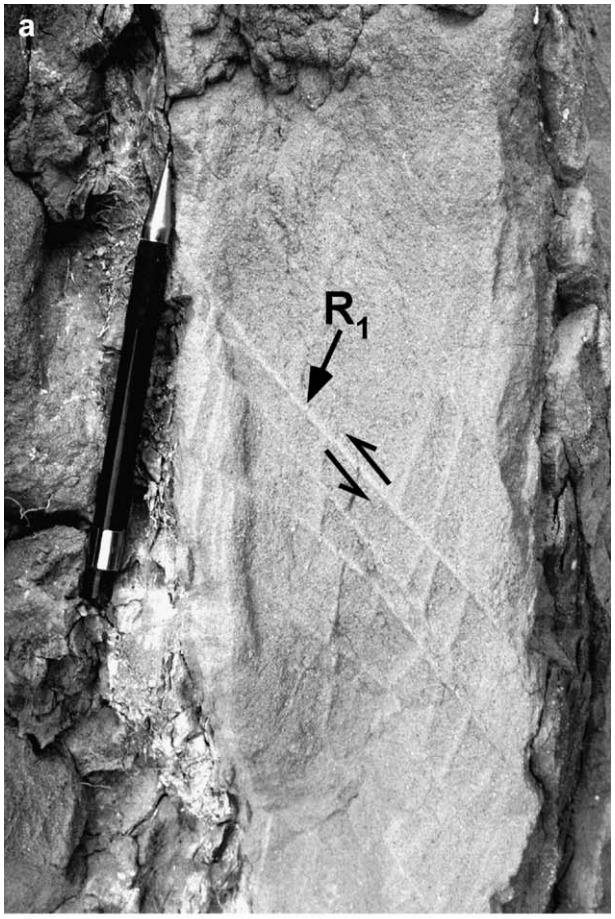

Fig. 3. Details of Santa Ana fault outcrop. (a) Individual and clustered (next to pencil) fault-parallel deformation bands offset by deformation bands in the R_1 orientation (see Fig. 4f). Pencil is 10 cm long. (b) Shear zone of coalesced deformation bands (DBSZ) separating footwall mixed zone from footwall damage zone. Foliated clay of fault core is visible to left of DBSZs. Relative movement in both photos is left (southeast) side down.

mentioned in the following descriptions are from figs. 7 and 10 of Heynekamp et al. (1999).

3.2.2.1. Upper Shooting Gallery—narrow fault (Fig. 5). At the top of the outcrop (Fig. 5a) the fault zone is less than 1 m wide and juxtaposes thickly bedded (>20 m) sediments with >50% clay in the hanging wall against thinner bedded (≤6 m) sediments with <50% clay in the footwall. Within the sands of the mixed zone are steeply dipping S- and C-surfaces defined by thin compositional bands. These are locally offset by C′-surfaces (Fig. 5b and d). Bedding is preserved within sigmoidal pods of sand (Fig. 5c).

3.2.2.2. Lower Shooting Gallery—intermediate width fault (Fig. 6). Several tens of meters below the upper outcrop, the fault zone is approximately 10 m wide and juxtaposes thickly bedded (several tens of meters) sediments with ≤20% clay in the hanging wall against thinner bedded (2–6 m) sediments with either ≤20% clay or >50% clay. Rotated and attenuated gravel beds, prominent in the cemented hanging-wall mixed zone, are commonly cut by R_1 and R_2 shears (Fig. 4). These are macroscopically ductile features that preceded cementation. There is no evidence of post-cementation fracturing. The tan medium-grained sand has an irregular but smoothly varying contact with the overlying red-tan clay-rich medium sand. There are three sets of deformation bands: a subvertical set, and two orientations that may represent a conjugate pair, with one member of the pair shallowly E-dipping, and the other dipping west ~45°. Sparse bedding laminae are evident between the deformation bands and are steeply dipping and subparallel to the clay-rich layers just above. The total strain accommodated by the array is small, as the offset along any one deformation band is no more than 2–3 cm.

3.2.2.3. Waterfall—wide fault (Fig. 7). Here the fault zone is ≥20 m wide and juxtaposes at least 10 m of sediment with ≤5% clay in the hanging wall against sediment with <20% clay in the footwall. Just east of the cross section shown in Fig. 7a are the clay core and cemented hanging-wall mixed zone, which are similar to those at the lower Shooting Gallery site. Both relict bedding (Fig. 7b) and evidence for grain-scale mixing (Fig. 7c) are present within the mixed zone. The latter includes sand and pebbles in a clay-rich matrix.

Features developed to varying degrees in mixed zones in all three outcrops include:

1. Compositional layers, which are generally much thinner (<<1 m) than bedding in the adjacent host sediment, slightly inclined and/or asymptotic to the fault core, and with a sigmoidal shape that records the down-to-the-east fault kinematics
2. Local preservation of sedimentary structures only within sandy lenses
3. Non-planar but geometrically smooth contacts between disparate sediment types

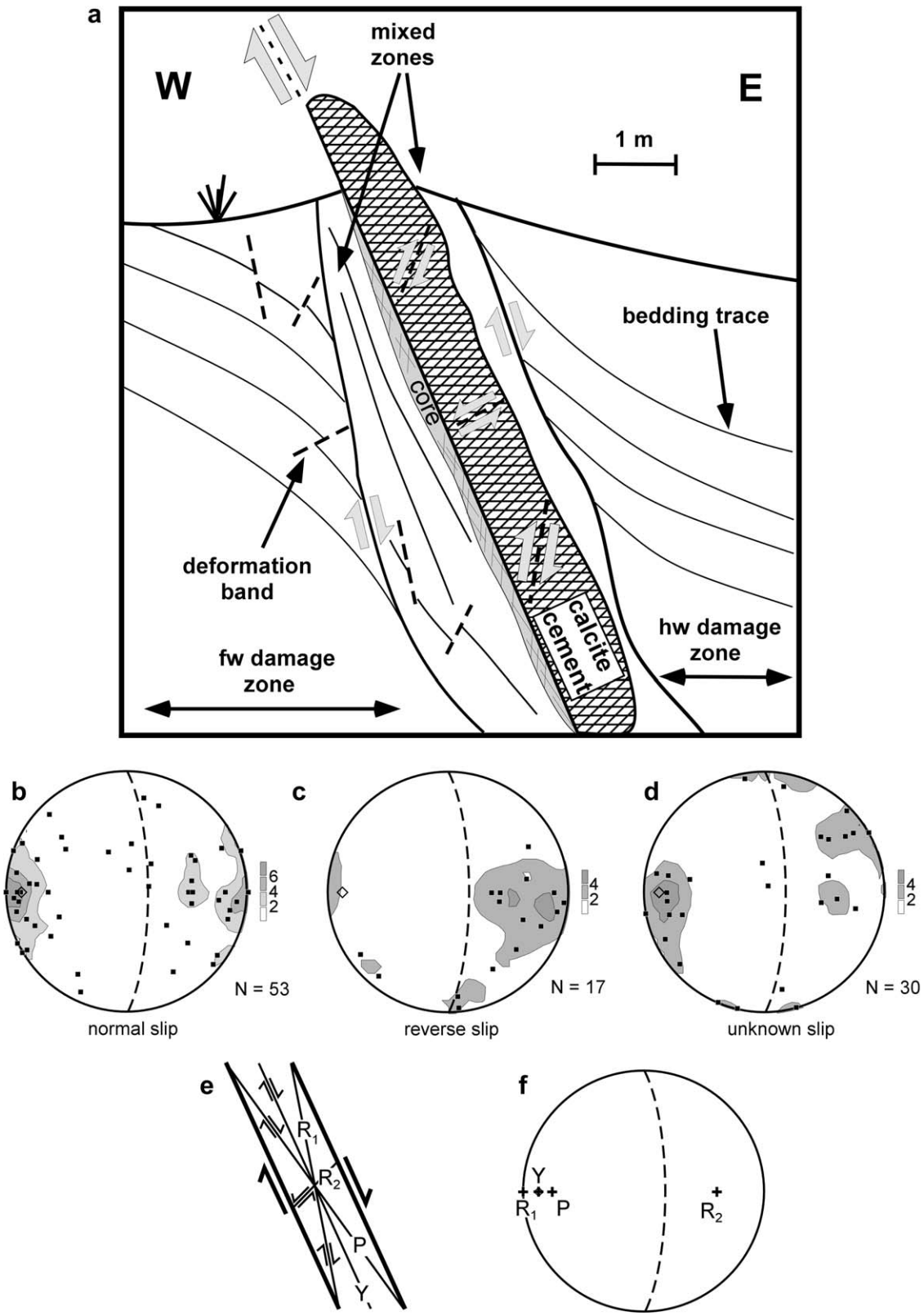

Fig. 4. (a) Schematic diagram of Sand Hill fault zone viewed to north showing architectural elements and typical locations and orientations of deformation bands. Includes data from (Heynekamp et al., 1999). Lower hemisphere equal-area plots of poles to: (b) normal slip deformation bands; (c) reverse slip deformation bands; (d) unknown slip deformation bands. Data compiled from 9 km traverse along Sand Hill fault. Fault strike at each outcrop rotated to 000° and plotted with average dip of 76° E (dashed great circle; open diamond is pole to fault). Data for each outcrop rotated with local fault trend, so that all deformation band orientations are shown with respect to the main fault orientation. Contours are in multiples of uniform distribution by the method of (Starkey, 1977). White area represents less than two times uniform distribution. (e) Orientations of and (f) poles to brittle shear zone structures, after Logan et al. (1992).

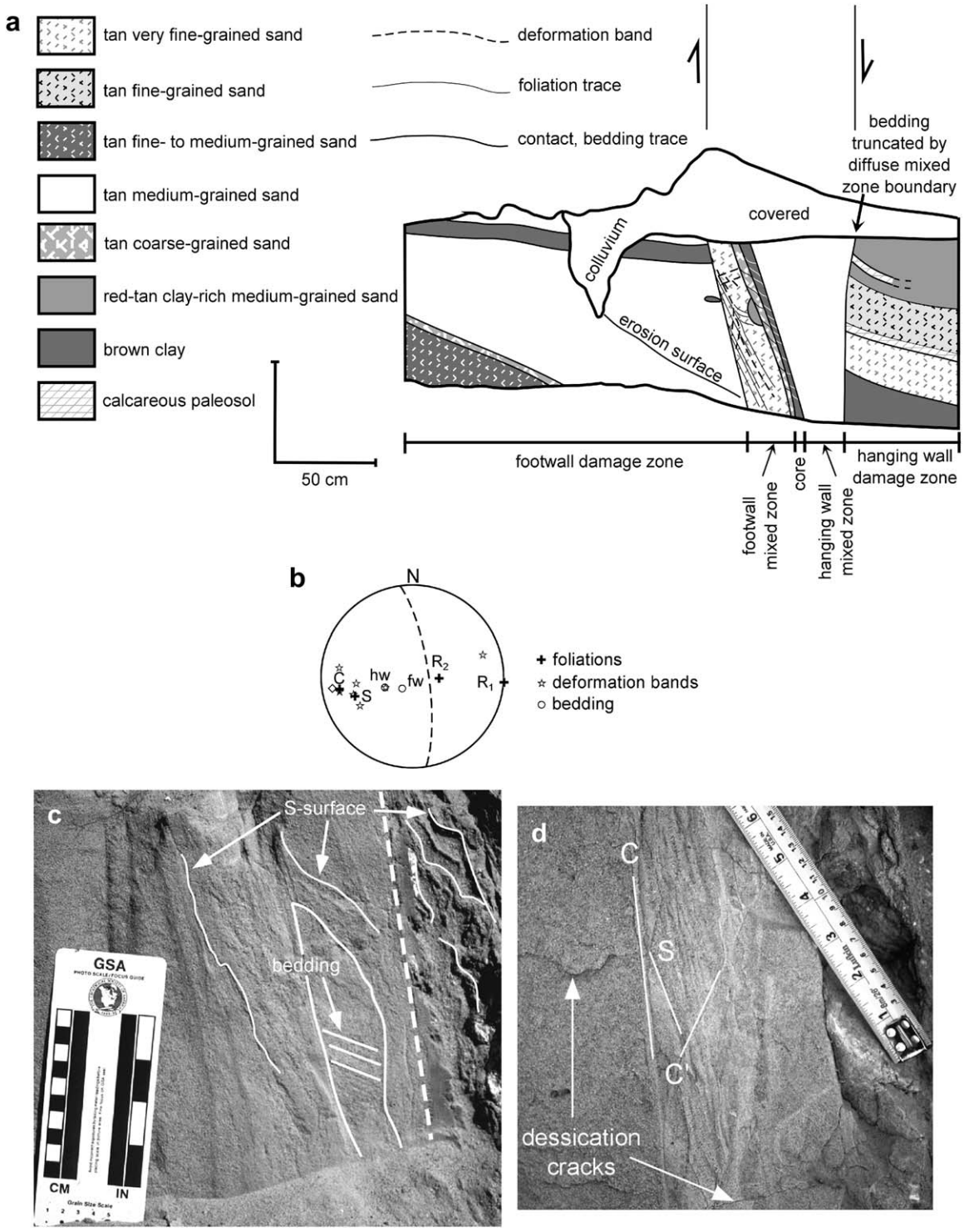

Fig. 5. (a) Cross-section of upper portion of Shooting Gallery outcrop. (b) Lower hemisphere equal area net plot of poles to planar structures at upper Shooting Gallery outcrop. Dashed great circle is contact between clay core and footwall mixed zone. (c) Foliations in footwall mixed zone. Dashed line is contact between clay-rich core and largely sand footwall mixed zone. Compositional foliations in sand and clay shown by curved white lines. Three straight lines indicate relict bedding within pod of coarse sand. (d) Compositional layers with S-, C-, and C′-surfaces indicated. Cracks are due to desiccation of clay-rich areas after outcrop excavation. Cross section and images viewed to north, with east (right) side down.

4. Sand foliations defined by variations in color, grain size, grain shape preferred orientation, and surface texture on excavated and brushed surfaces
5. Down-dip lineations on foliation surfaces defined by grain alignment
6. Evidence of grain-scale mixing of sediment
7. Steeply dipping clay beds in the mixed zones that thin down-dip, and exhibit variable foliation development
8. Overprinting of foliated sands by deformation bands

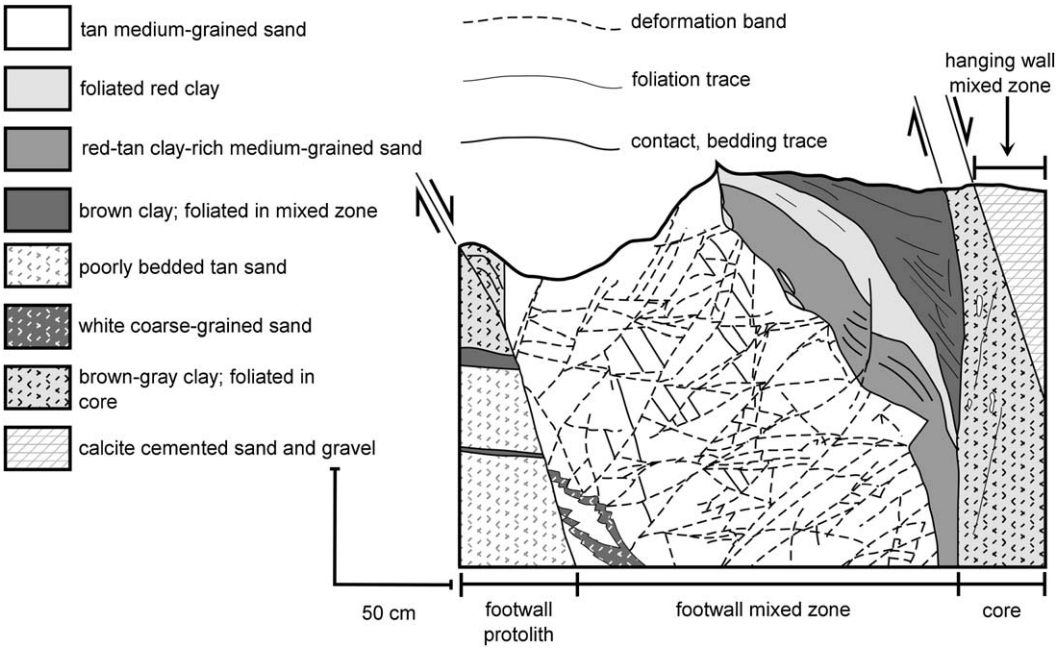

Fig. 6. Cross section of lower portion of Shooting Gallery outcrop, viewed to north. Note that the damage zone is essentially nonexistent.

9. Networks of deformation bands within the mixed zones (Figs. 2 and 6)—in contrast, deformation band networks in the damage zones are geometrically much simpler or nonexistent regardless of displacement magnitude (Figs. 2 and 7a)
10. Deformation band shear zones of variable width at sand-on-sand mixed zone–damage zone contacts

These features are ubiquitous in faults cutting poorly lithified sediments of the Rio Grande rift. Similar features have been observed in the San Ysidro fault of the northern Albuquerque Basin (J.S. Caine, personal communication, 2003) and in faults in the Espanola Basin of northern New Mexico (observations by the first author of faults mapped by Koning (2003) and Read et al. (2005)).

4. Microstructural observations

4.1. Sample description and preparation

We sampled several outcrops of the Sand Hill fault. After vacuum impregnation with low viscosity epoxy, 53 oriented thin sections were prepared. Even with care in sampling and preparation, grain plucking is a problem in most of the undeformed sediment and deformation band shear zone sections, although somewhat less so in mixed-zone sand sections.

Preliminary observations were made with the petrographic microscope. Then the best preserved samples from the Waterfall outcrop of undeformed footwall sand, a transposed layer within the mixed zone, a pod of sand in the dominantly clay core zone, and a deformation band shear zone were examined with the electron microprobe in back-scattered electron mode. Although the total amount of strain accommodated is unknown, the mixed-zone sand sample represents a lesser degree of strain localization than either the core as whole or the deformation band shear zone.

Thin sections of the undeformed sediment sample were prepared in two orientations: A—perpendicular to approximately horizontal bedding (i.e., vertical), and B—parallel to bedding (Fig. 8). Sections from the fault zone were prepared in three orientations (Fig. 9a): A—parallel to either compositional layering, planes of deformation bands, or foliation, and approximately fault-parallel. The section long axis is parallel to the down-dip sand lineation; B—perpendicular to both the fault and foliation with the long axis of the section vertical and parallel to the down-dip lineation; and C—horizontal, and perpendicular to the fault, the foliation, and the down-dip lineation.

4.2. Grain shape preferred orientations

To quantitatively assess foliation and lineation, evaluate kinematics of different fault-zone elements, and constrain deformation mechanisms, shape preferred orientations of grains were measured using image analysis software. We characterized four to eight non-overlapping back-scattered electron images from each thin section. The grayscale images were processed to pure black (grains) and white (background) images and touching grains were separated manually in each image by adding white pixels. The best-fitting ellipse to each of the larger grains was calculated, and the ellipse axial ratio and long-axis length and orientation were recorded. Partially plucked grains, clay, small fragments derived from cataclasis of larger grains, and grains truncated by the edge of the image were not measured. The number of grains measured in each image ranged from about 30 to more than 100, depending

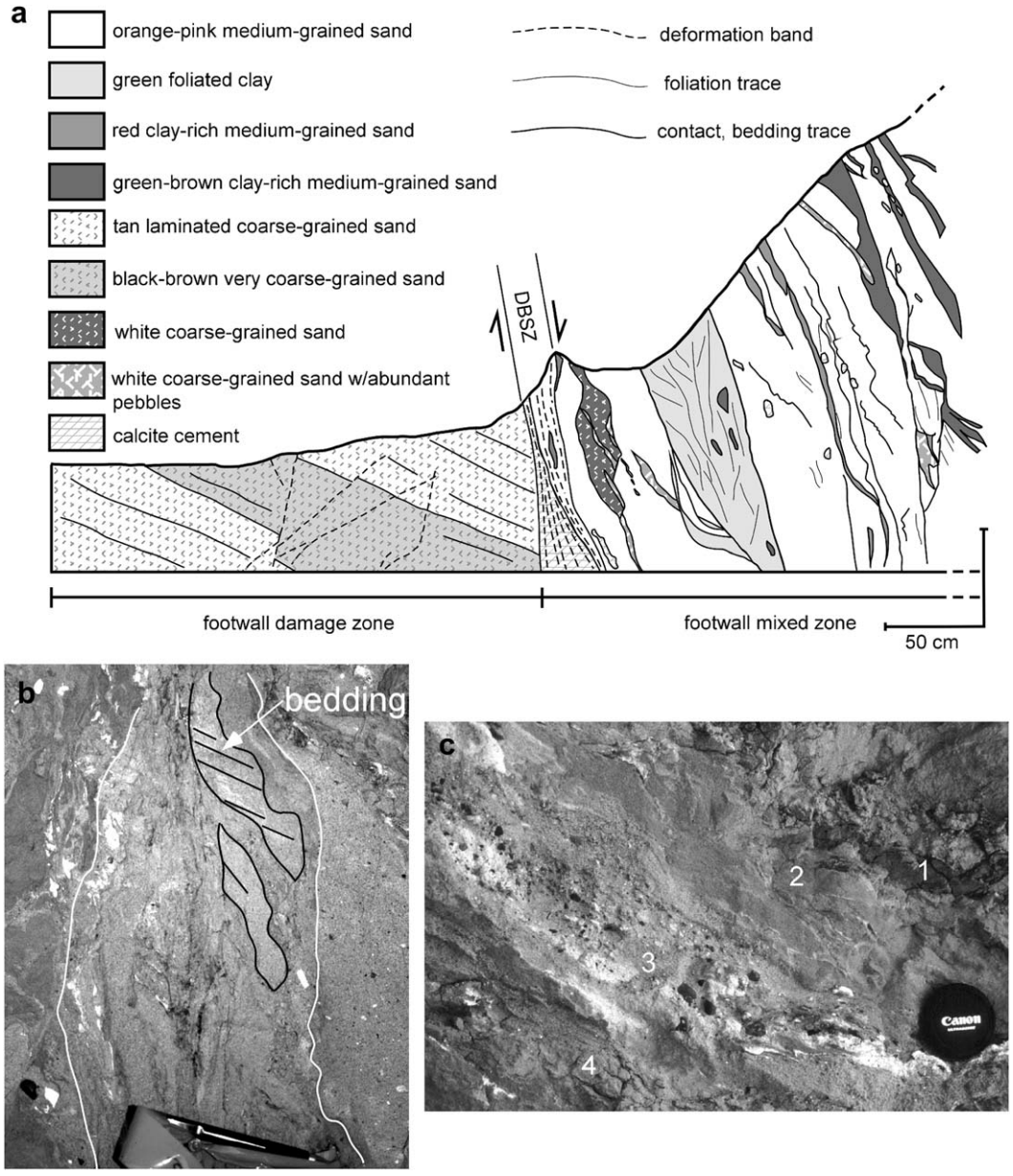

Fig. 7. (a) Cross section of west half of Waterfall outcrop. The large lenticular pod of clay pinches out abruptly both up and down-dip. Fault core is east of mapped portion of outcrop. (b) Compositional banding and foliation. White lines bound central high strain zone, with red, clay-rich sand with tan sand inclusions on left and tan coarse sand on right. Black lines delimit pods of medium sand with relict bedding separated by sheared zone of coarse sand. Pencil is 10 cm long. (c) Mixing of (1) sandy clay, (2) clay-rich sand, (3) coarse sand with pebbles, and (4) clay-rich sand. Contacts interfinger and are gradational over ~1 cm. Note streaks of unit 3 within unit 2. White patches are micritic calcite cement. (a) and (b) viewed to north, with east (right) side down, (c) is viewed to northeast, oblique to fault.

on average grain size. Grains with aspect ratios <1.4 were discarded, as their orientations cannot be determined robustly (Shelley, 1995; Cladouhos, 1999). The data are presented in Figs. 8 and 9 and Table 1.

All samples show statistically significant grain-shape preferred orientations. The shape preferred orientation in the undeformed sample—inferred to record the orientation of the current at the time of deposition—is oriented NNE–SSW within the plane of bedding (Fig. 8). In A (fault parallel) sections from the deformed samples (Fig. 9), shape preferred orientations are varied within the foliation plane, with the deformation band shear zone sample having a down-dip alignment similar to sand lineations (aligned sand grains) visible on foliation planes in outcrop. The grain shape preferred orientation in the fault-parallel (A) section from the mixed zone is neither down-dip nor strike-parallel (Fig. 9b, left column), whereas that in the fault-parallel (A) section from the core zone sand is also moderately inclined, but poorly developed (Fig. 9c, left column).

In B (fault-normal, lineation-parallel) sections, all deformed samples have strong shape preferred orientations inclined to the fault, dipping 40° to 55° from horizontal (Fig. 9, middle column), with the deformation band shear zone sample having the steepest dip. These dips are equal to

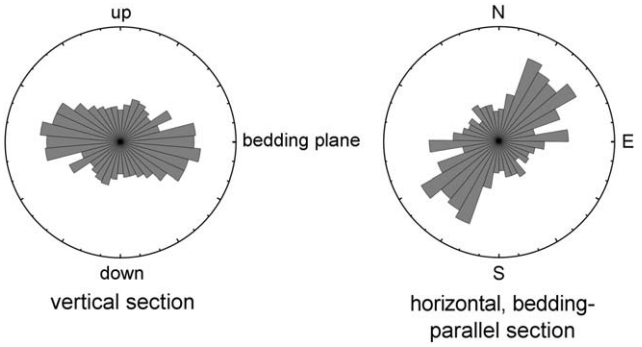

Fig. 8. Rose diagrams of orientations of grain long axes in two perpendicular sections of undeformed sand. Number of data points and statistics are presented in Table 1.

or shallower than that of the local compositional layering or local shear zone boundaries (Table 1), and thus the shape preferred orientations are similar in orientation to a P-foliation or S-foliation (cf. Rutter et al., 1986; Logan et al., 1992). In contrast, the shape preferred orientation in the undeformed sample is symmetric about bedding, suggesting that the shape preferred orientation in the deformed samples is an inclined foliation, and not passively rotated bedding. The angle of inclination of the shape preferred orientations relative to the fault as a whole (<30°) is similar to that reported by Cladouhos (1999) for survivor grains in clay-rich fault gouge.

In the C (fault-normal, lineation-normal) section, the shape preferred orientation of the DBSZ sample is aligned normal to the foliation (Fig. 9d, right column). Taken together, the three mutually orthogonal shape preferred orientation measurements from the deformation band shear zone define a fabric with approximately monoclinic symmetry that records the bulk kinematics of the fault zone (dip-slip motion). The grain shape preferred orientation in the subhorizontal, fault-perpendicular (C) section from the mixed-zone, however, is aligned parallel to fault strike (Fig. 9b, right column). Thus, the three mutually orthogonal shape preferred orientation measurements from the mixed zone do not correlate with the bulk kinematics of the fault zone (i.e., they do not record pure dip-slip motion).

5. Discussion

Structures from the outcrop to the grain scale form a physical record of the mechanical response of these poorly lithified sediments to faulting. This record includes a unique ensemble of features, many of which are similar to those found in ductile shear zones deformed in general shear (e.g., S-, C-, and C′ surfaces, sand lineations, compositional banding foliation), but others familiar from faults in fully lithified rock (deformation bands, clay-rich fault cores). A systematic consideration of factors leading to the formation of these structures follows, ending with the development of a conceptual model describing the mechanical evolution over time and space of the mixed zone, the key architectural element that is distinct to these faults in sediment. This model is very different from an earlier one proposed by Heynekamp et al. (1999), which the present observations demonstrate is incorrect.

5.1. Incorporation of sediment into the fault zone

Where a normal fault cuts heterogeneous layered sequences with competency contrasts, such as the interbedded sand and clay of the Santa Fe group, the fault assumes a steeper dip in the stronger layers (in this case, sand) and a shallower dip in the weaker layers (clay) (Peacock and Sanderson, 1992). This results in vertically segmented faults with steps at lithologic/competency contrasts (Childs et al., 1996a). Destruction of these steps by tip-line bifurcation and asperity bifurcation incorporates wall rock into the fault zone and enhances its internal complexity (Childs et al., 1996b; Watterson et al., 1998) (Fig. 10).

There is no direct evidence for bifurcation processes at the outcrops in this study, but there are significant vertical changes in the dip of minor faults at sand-clay stratigraphic contacts at the Santa Ana fault (Fig. 2) and in small faults adjacent to the Sand Hill fault. There are three large fault horses (several to tens of meters in size in map view and cross section) along the trace of the Sand Hill fault (Heynekamp et al., 1999), which we infer to have formed by bifurcation. The Calabacillas fault a few km east of the Sand Hill fault shows evidence for bifurcation processes (fig. 6 in Doughty, 2003). In addition, the contrasts in the Waterfall and Shooting Gallery sites are generally consistent with bifurcation processes having been operative. For example, Watterson et al. (1998) showed that the contribution to fault-rock thickness by asperity bifurcation increases with increasing bed thickness and rotation. The widest portion of the Sand Hill fault includes the Waterfall site, which also has the widest footwall mixed zone. Here the footwall stratigraphy has thicker sand beds and dips more steeply into the fault zone than at the Shooting Gallery site (Heynekamp et al., 1999). We therefore infer that sediment was initially incorporated into the mixed zones at least in part by bifurcation processes.

5.2. Ductile deformation and particulate flow

Several lines of evidence, at both outcrop and thin section scales, indicate that deformation by penetrative particulate flow is important in the formation of mixed zones once sediment begins to be deformed within the fault zone.

5.2.1. Geometry of compositional layering and shear zones

Previous studies have shown that material incorporated into fault zones by bifurcation processes includes subangular to rounded blocks surrounded by gouge and lenses bound by slip surfaces, and exhibits varying degrees of internal deformation (Childs et al., 1996b; Childs et al., 1997; Foxford et al., 1998; Watterson et al., 1998; Aydin and Eyal, 2002). Mixed zones represent a variation on this pattern, containing a gradation from pods of relatively intact sediment (fig. 5c in Heynekamp et al., 1999) to attenuated, foliated, and mixed material

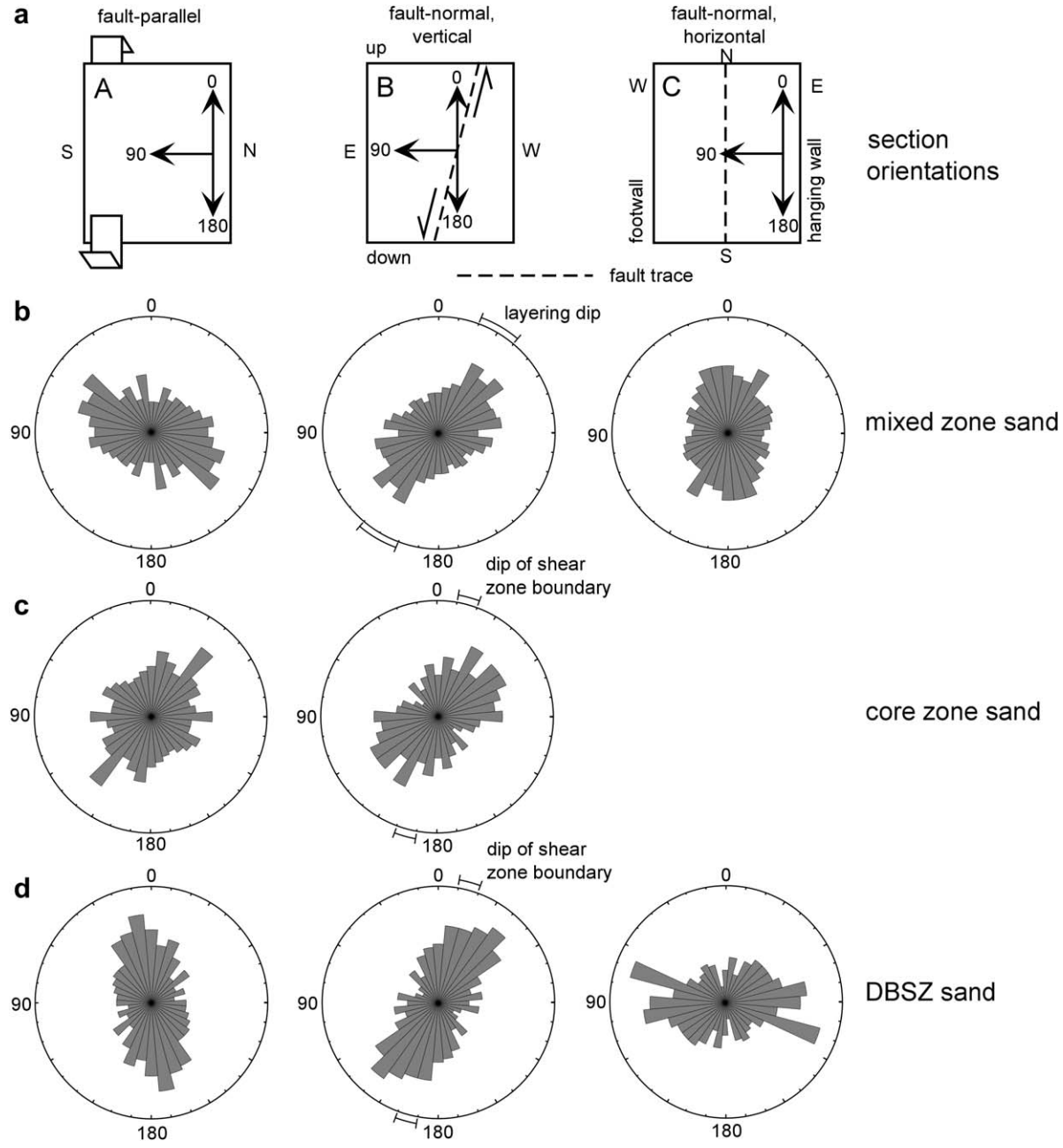

Fig. 9. Rose diagrams of orientations of grain long axes in mutually perpendicular sections of deformed sands. Numbers of data and statistics are presented in Table 1. (a) Orientation schemes for A, B, and C sections relative to fault. Data from sections of a given orientation are arranged in columns below the orientation diagrams. (b) Mixed-zone sand. (c) Core-zone sand. (d) Deformation band shear zone (DBSZ) sand.

(with or without compositional banding) in which the compositional layers commonly resemble ductile structures from deep crustal shear zones (Fig. 7, cf. Goodwin and Tikoff, 2001). Within the large displacement (up to 600 m) Sand Hill fault, such variation may represent a gradient of time spent within the fault zone, and/or amount of deformation, and/or variations in cohesion and consolidation state (see Section 5.4), and/or competency contrast between sand-rich and clay-rich material. Perhaps the relatively intact blocks were more recently incorporated into the fault and the highly deformed mixed zone material has experienced a longer history of deformation. However, elongate, fault-parallel and penetratively foliated sandy mixed zones in the Santa Ana fault suggest that highly deformed mixed zones can form with throw as low as 10 m.

Nonplanar but smooth contacts between units of differing lithology (and probably competency, Fig. 7) are consistent with penetrative particulate flow within the mixed zones. This type of macroscopically ductile deformation could prevent significant strain or displacement discontinuities across lithologic contacts and the ensuing formation of voids or fractures. Rather than discrete displacement surfaces, high strain zones between disparate sediment types have curviplanar and macroscopically ductile morphologies (Fig. 7b).

Table 1
Sample descriptions and grain-shape preferred orientation data

Description	Orientation of thin section[a]	n[b]	Mean[c] ± interval[d]	Dip of local layering or shear zone boundary
Footwall sediment	Within bedding plane	401	049° (NE) 16°	
Footwall sediment	Normal to bedding plane	507	99° (~horiz.) ± 19°	
Mixed zone sand	**A** (fault and foliation //, lineation //)	460	071 ± 24°	
Mixed zone sand	**B** (fault and foliation ⊥, lineation //)	493	130 ± 22°	140–160°
Mixed zone sand	**C** (fault and foliation ⊥, lineation ⊥)	548	178 ± 25°	
Core zone sand	**A** (fault and foliation //, lineation //)	396	145 ± 50°	
Core zone sand	**B** (fault and foliation ⊥, lineation //)	241	133 ± 27°	160–170°
DBSZ[e] sand	**A** (fault and foliation //, lineation //)	229	010 ± 23°	
DBSZ sand	**B** (fault and foliation ⊥, lineation //)	274	155 ± 16°	160–170°
DBSZ sand	**C** (fault and foliation ⊥, lineation ⊥)	271	096 ± 24°	

[a] ⊥ = normal, // = parallel; see also Fig. 9.
[b] Number of measurements.
[c] Mean direction of grain shape preferred orientation; reference scheme for fault samples in Fig. 9.
[d] 95% confidence interval about mean direction.
[e] Deformation band shear zone.

5.2.2. Local preservation of bedding

Steeply dipping bedding laminae are locally preserved between deformation bands at the lower Shooting Gallery site (Fig. 6). The small displacements involved in the formation of these deformation bands could not accommodate, and therefore did not cause, the rotation of the bedding to its current steeply dipping orientation. The sparse preservation and rotation of bedding probably records penetrative deformation that largely disaggregated the sediment and destroyed the sedimentary structures.

The pod including relict bedding in Fig. 7b is irregular in shape and contained within a high strain zone. Unlike boudinaged or brecciated beds surrounded by gouge in faults in lithified rock (e.g. Aydin and Eyal, 2002; Cowan et al., 2003), the pods of bedding are not bound or cut by fractures or joints. They pinch out in trails of sand that extend up and down dip. We infer that the sigmoidal shape of the pods is due to progressive, grain-scale erosion of sediment from their margins by particulate flow in the shear zone with a significant simple shear component.

5.2.3. Grain shape preferred orientations

As noted above, the shape preferred orientation in the undeformed sample is symmetric about bedding. The angular relationship between the shape preferred orientations in the deformed samples and the boundaries of local compositional layers or shear zones (Fig. 9, middle column, and Table 1) suggests that these shape preferred orientations record a penetrative, inclined foliation, and not just passively rotated bedding.

In the B sections, the shape-preferred orientations record the fault kinematics in all of the deformed samples, and perhaps record the varying degrees of strain localization and/or total strain. Although statistically not significant, the shape preferred orientation in the deformation band shear zone dips more steeply (hence, forms a smaller angle with the fault) than that of the mixed and core zone samples. This is consistent with greater strain localization and/or total strain in the deformation band shear zone sample as compared to the other deformed samples, and with the greater intensity of cataclasis in the deformation band shear zone (cf. Rawling and Goodwin, 2003).

Possible explanations for mixed zone and core zone deviations from the kinematics recorded by the grain shape preferred orientation within the deformation band shear zone are:

1. the deformation band shear zone experienced greater strain;
2. the deformation band shear zone represents a different portion of the fault zone deformation history (see Section 5.4); or
3. the mixed zone and core zone samples record local oblique slip. The mixed and core zone shape preferred orientations may record local kinematic variations caused by nonplanar shear zone boundaries or sediment heterogeneity, which could result in, for example, local development of oblique-slip or triclinic shear.

Taken together, the grain shape preferred orientation data imply non-plane strain that is penetrative at the grain scale, due to complex spatial and/or temporal patterns of deformation within the fault zone.

5.3. Structural development of mixed zones

Our observations do not require any mechanisms for initial incorporation of sediment into the fault zone other than those that have been previously documented for normal faults in lithified rock, although others are certainly possible. Continued slip on the fault strains the blocks and lenses of incorporated sediment, which deform by disaggregation at the grain scale and penetrative particulate flow facilitated by cataclasis (Rawling and Goodwin, 2003), rather than by the formation of shear fractures and joints typical of faults in lithified rocks. Miller (1996), Chester and Chester (1998), Cladouhos (1999), and Cowan et al. (2003) all documented macroscopically ductile deformation and mixing within clay-rich gouge and cataclasite in faults in crystalline and lithified sedimentary rocks. However, all of the faults they studied had undergone very

large displacements and the fault gouge was derived from crystalline and lithified sedimentary rocks by brittle deformation and alteration caused by water-rock interaction. In contrast, due to the poorly lithified and inherently weak nature of the Santa Fe group sediments, deformation in the mixed zones was accomplished by sediment disaggregation and penetrative particulate flow at displacements as small as 10 m.

Heynekamp et al. (1999) proposed that damage zones formed early in the evolution of the Sand Hill fault zone and continued to widen and increase in complexity until a thoroughgoing clay core developed, facilitating localization of deformation. Significantly, the detailed outcrop mapping and microstructural observations presented here do not support this model of early development of damage zones. The well-developed mixed zone and poorly developed damage zone in the small-displacement Santa Ana fault indicate that mixed zones can form at relatively small displacements prior to extensive damage zone development. In addition, consistent overprinting of macroscopically ductile structures by deformation bands indicates that the latter represent a later, more localized style of deformation that postdates mixed zone formation. They are present in deformed mixed-zone sands that show evidence of penetrative particulate flow (Figs. 3 and 6), so they must have formed after this penetrative deformation occurred, as such deformation would distort their planar to curviplanar geometry or erase them completely. DBSZs forming mixed zone–damage zone contacts truncate structures in both architectural elements. This truncation of mixed-zone structures suggests that these DBSZs at least partly postdate the development of mixed zones, although we have found no definitive cross-cutting relationships confirming this.

If mixed-zone sediment is derived from bifurcation processes, once an extensive mixed zone forms, the largest geometric irregularities along the fault may have been planed off (Fig. 10). Formation of a mechanically weak clay core, combined with the development of an approximately planar zone of faulted and deformed material should promote subsequent localization of deformation. The deformation bands along the Sand Hill fault largely record plane strain related to dip-slip movement along the fault (Fig. 4). This contrasts with the more complex and heterogeneous strain field recorded by the grain shape preferred orientations (Fig. 9). If damage zones and their component deformation bands represent a later stage of fault zone evolution, they may be accommodating relatively small strains within the hanging wall and footwall sediments as they are continually juxtaposed across a broadly planar fault core.

5.4. Mechanical considerations

5.4.1. Consolidation state and deformation style

The consistent overprinting relationships we observe in outcrops of both the Santa Ana and Sand Hill faults indicate a transition from distributed, penetrative particulate flow with little cataclasis except in localized shear zones (Rawling and Goodwin, 2003) to localized cataclastic deformation (deformation bands and deformation band shear zones). As these two faults have throws that differ by hundreds of meters, this transition is probably not a function of displacement. We infer that such different deformation styles result from a change in the mechanical response of the sediment-fault system to applied tectonic stresses. We interpret this transition with the theory of critical state soil mechanics, which describes the relations between stress and volumetric strain of a body of unlithified or poorly lithified sediment during burial and compaction, exhumation and unloading, and shear deformation (Jones, 1994; Karig and Morgan, 1994). Within this framework, progressive changes in the stress–strain state of a body of sediment are typically illustrated in mean stress–differential stress–porosity space (Fig. 11a).

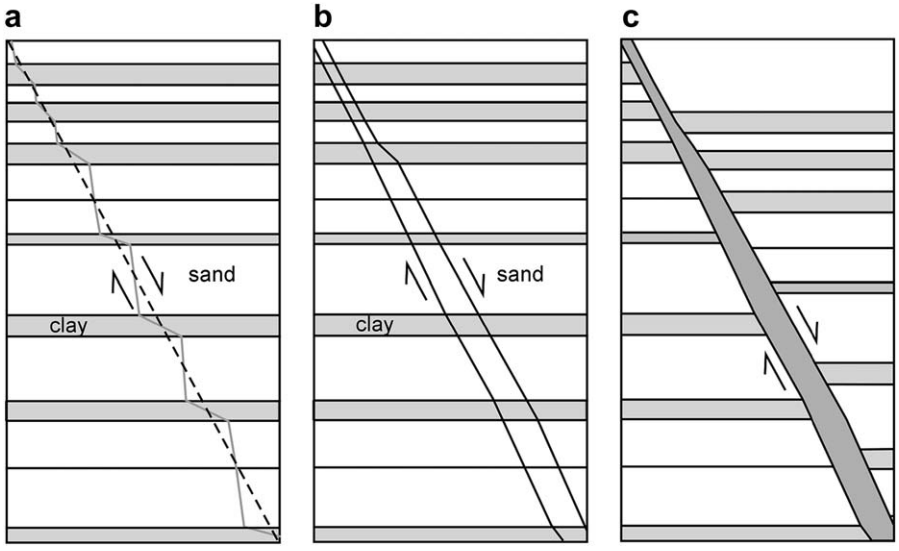

Fig. 10. (a) Schematic diagram of fault cutting interbedded sand and clay. Solid gray line shows deflection of fault trace due to competency contrasts. Dashed line is average fault dip. (b) Solid lines bound material enclosed within dashed and gray lines in (a) which could potentially be incorporated into the fault by tip line and asperity bifurcation and smearing of clay. (c) Gray area is nascent mixed zone formed from bifurcation processes and subsequent particulate flow. Core zone would lie approximately along the midline of the mixed zone.

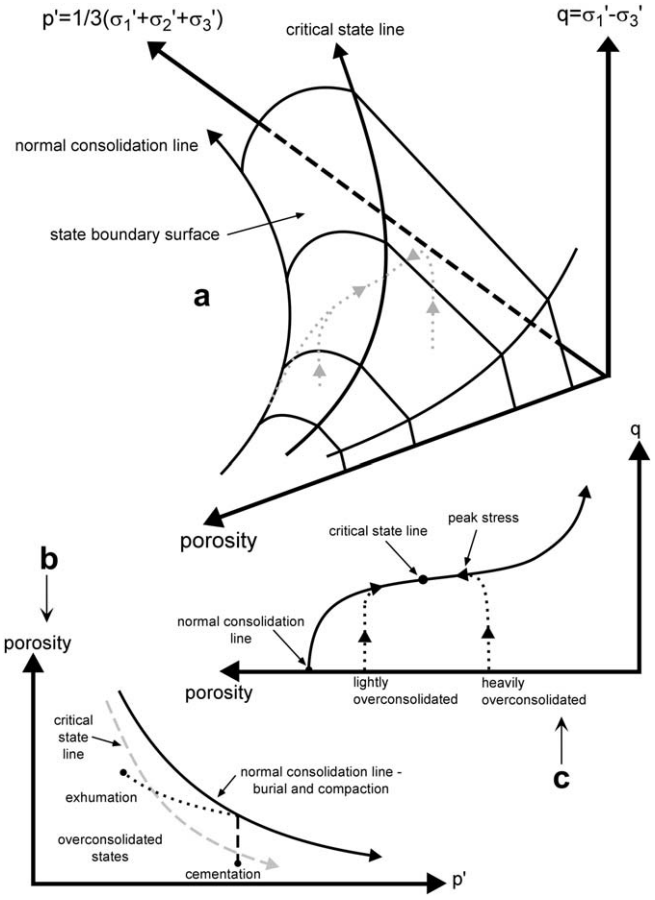

Fig. 11. (a) Generalized critical state diagram in mean stress (p′)–differential stress (q)–porosity space showing idealized, partially drained, stress–strain paths of tectonically deformed sediment (gray dashed lines). Perfectly drained stress–strain paths plot within planes parallel to $q = 3p'$ and undrained stress–strain paths plot within planes of constant porosity. (b) Projection onto plane $q = 0$. Normal consolidation line approximates burial-induced compaction of sediment. Dashed black lines show subsequent overconsolidation due to exhumation or cementation. Projection of critical state line divides fields of lightly (right) and heavily (left) overconsolidated sediment. (c) Slice through state boundary surface parallel to plane $p' = 0$. Stress–strain paths of tectonic deformation terminate at the critical state line, where deformation proceeds at constant porosity and differential stress.

We infer that the initial, distributed, macroscopically ductile style of deformation took place when the mixed zone sediment was normally consolidated (Fig. 11b). In this state, the sediment had never experienced greater effective stresses than the prevailing ambient conditions (Jones and Addis, 1984, 1986). Shear deformation of normally consolidated sediments results in particulate flow and a decrease in porosity (compaction). The sediment will compact and strain harden until it attains a set of stress and porosity conditions known as the critical state, at which point the sediment can theoretically deform indefinitely at constant stress and porosity (Jones and Preston, 1987; Jones, 1994) (Fig. 11c). In reality, deformation at the critical state continues until the driving stresses dissipate, deformation mechanisms change, or geometric boundary conditions preclude further deformation. Compaction and strain hardening may promote the spread of deformation into adjacent sediment (Moore and Byrne, 1987).

Sediment is said to be overconsolidated if the ambient effective stress decreases below the maximum stress to which it has been subjected (Atkinson and Bransby, 1978; Jones and Preston, 1987) (Fig. 11b). During shear of strongly overconsolidated sediments, the material strain hardens until a peak stress is attained, followed by strain softening (Bishop, 1975; Skempton, 1985) (Fig. 11c). The post-peak strain-softening corresponds to spatial localization of deformation and the formation of discrete shear zones, within which material continues to deform at the critical state, whereas material outside the shear zone is effectively unloaded and does not deform further (Ellen and Fleming, 1987; Bolton et al., 1998). Again, deformation at the critical state within the shear zone continues until the driving stresses dissipate, deformation mechanisms change, or geometric boundary conditions preclude further deformation. We infer that, in our case, the discrete shear zones are deformation bands, which overprint the macroscopically ductile structures in the mixed zones.

The critical state theory does not account for microscopic deformation mechanisms, specifically cataclasis. Been et al. (1991) performed compression tests on a dominantly quartz sand and observed that at mean stresses above 1 MPa, the occurrence of cataclasis lowers the porosity at the critical state (figs, 9, 11, and 12 of Been et al., 1991). However, the two general types of behavior described above still occurred, depending on the initial porosity and stress state of the sand relative to the critical state, i.e., whether the sediment was initially normally consolidated or overconsolidated (Fig. 11b; see also Moore and Byrne, 1987 and references therein).

Mair et al. (2000) experimentally studied the sequential formation of deformation bands in lithified porous sandstones and observed that the initial formation of a fault composed of deformation bands is accompanied by a stress drop, i.e., strain softening. Further shortening of the sample proceeded at approximately constant stress. Post-failure deformation at constant stress or continued strain-softening is seen during brittle deformation of porous sandstones at confining pressures <50 MPa (e.g. Menéndez et al., 1996; Wong et al., 1997). Lithified sandstones are sediment overconsolidated via mechanical compaction and/or cementation (see Section 5.4.2) and their macroscopic deformation behavior is consistent with the predictions of the critical state theory (Wong, 1990).

Aydin (1978) and Aydin and Johnson (1978) studied zones of deformation bands in lithified porous sandstones and documented a correlation between the number of bands in a shear zone and the offset across the zone. Because each individual band accommodated little displacement, these authors suggested that they are strain-hardening phenomena. Proceeding from this field interpretation, Mair et al. (2000) speculated that the strain accumulation at constant stress documented by their experiments recorded the sequential growth of individually strain-hardening deformation bands following sample failure, where a new deformation band initiated at the exact moment a previous one locked up.

We observe deformation band shear zones that clearly accommodated greater offset than individual bands (Fig. 7a). However, in a study of poorly lithified sediments of the Santa

Fe Group, Herrin (2001) observed no correlation between the number of deformation bands within, or thickness of, deformation band shear zones, and the displacement across the deformation band shear zones. This casts doubt on whether cessation of movement on individual bands is solely due to strain hardening. We suggest that differences in the elastic properties (Haneberg, 1999; Wibberly et al., 1999) and/or grain scale deformation mechanisms (Rawling and Goodwin, 2003) between poorly lithified sediment and lithified sedimentary rock, and in general the influence of loading history, strain rate, and boundary conditions and/or imposed displacements (cf. Tikoff and Wojtal, 1999) may all influence the termination of slip in deformation bands.

Deformation bands in argillaceous sediments in the Nankai accretionary prism, southwest Japan have been interpreted as compactive shear bands that formed in normally consolidated sediments early in the deformation history (Ujiie et al., 2004). We feel that this interpretation can be excluded for the faults in the present study based on the overprinting relationships and evidence for early mixed zone development in the Santa Ana fault.

5.4.2. Changes in consolidation state

There are several ways in which changes in consolidation state may be induced. The first three processes described below are all probably important to some degree, and should act in concert to promote localization of deformation and formation of discrete shear zones such as deformation bands.

The majority of the observations from the Sand Hill fault are from the well-exposed footwall. The footwall and footwall mixed zones have been exhumed a couple of hundred meters, assuming that slip is localized within the fault core once it forms. The sequence of structures within the footwall mixed zone may reflect the effects of decreasing confining pressure and progressive overconsolidation due to footwall exhumation (Karig, 1986; Bolton et al., 1998) (Fig. 11).

The tectonic compaction of normally and lightly overconsolidated sediments during deformation is, in effect, a shear-induced overconsolidation. This is because after the faulting event, the deformed material has a lower porosity than the undeformed sediment outside the fault zone (Fig. 11c).

Spatially heterogeneous permeability distributions within the fault zone (Sigda et al., 1999; Rawling et al., 2001) can potentially inhibit drainage and allow pockets of elevated pore pressure to develop, which would tend to locally reduce the effective mean stress and induce an overconsolidated state. This process should act in concert with tectonic compaction to promote localization of deformation and formation of discrete shear zones such as deformation bands.

The effect of overconsolidation can be achieved by cementation, which lithifies and hardens the sediment relative to adjacent uncemented material (Fig. 11b). However, cementation is absent in the Santa Ana fault. In the Sand Hill fault there is no evidence that, where locally cemented, the hanging wall mixed zone underwent any post-cementation deformation, and cementation elsewhere is patchy and not pervasive. It is absent completely in many areas that show the relationships we describe. Therefore, it is not possible that the overprinting relationships are due to cementation affecting the consolidation state of the sediment.

The relative timing of formation of deformation band shear zones at mixed zone–damage zone contacts is uncertain. Cataclastic deformation in deformation band shear zones is much more intense than within adjacent mixed-zone sands (Rawling and Goodwin, 2003). If deformation band shear zones formed contemporaneously with mixed-zone structures, the more intense cataclasis may be because deformation band shear zones are high-strain zones and experienced higher strain rates. Conversely, if deformation band shear zones formed after the mixed-zone structures, the increased intensity of cataclasis may at least partly be due to a change in consolidation state.

In sum, given reasonable inferences on the consolidation history of the faulted sediments, the deformation style and overprinting relationships we observe in the faults in this study are consistent with the predictions of critical state theory. Confirming this interpretation would require an experimental program to determine preconsolidation stress and its relation to failure mode during shear deformation (localized vs. distributed) for a suite of samples collected within and adjacent to these faults.

6. Conclusions

We have used field and microstructural observations from normal faults cutting poorly lithified sediments of the Santa Fe Group of the Rio Grande rift, New Mexico USA, to document the development of mixed zones. In contrast with the fault zone evolution model of Heynekamp et al. (1999), we infer that initiation of mixed zones can occur very early during fault-zone evolution and need not be preceded or accompanied by extensive damage-zone development. We infer that sediment is incorporated into a given fault zone by bifurcation processes, and additional sediment may be incorporated throughout the movement history of the fault. Both the macro- and microscale observations indicate that initial deformation within the mixed and core zones in these faults was accomplished by penetrative particulate flow with subordinate cataclasis (cf. Rawling and Goodwin, 2003). Progressive deformation within mixed zones resulted in transposition of bedding into compositional and grain shape preferred orientation foliations and the development of local, macroscopically ductile, high-strain zones.

Ultimately, the style of deformation changed, and ductile structures were overprinted by deformation bands, which are a product of localized cataclastic deformation. This transition is consistent with the burial and exhumation history of the Sand Hill fault and progressive overconsolidation, probably due to a combination of tectonic compaction and unloading. These observations suggest that mixed zones in general may be preserved and overprinted by post-lithification deformation, recorded by deformation bands and/or discrete fractures.

Our observations indicate that mixed zones can initiate early in the deformation history of a given fault zone. In a region undergoing sedimentation and subsidence, growth faults

may form and remain active as they are buried. With burial, compaction, and lithification of the sediment into rock, early-formed mixed zones may be preserved and/or overprinted with macroscopically brittle structures. Post-lithification deformation likely would be localized in the form of relatively narrow cataclastic shear zones, discrete fractures, and fracture networks. It is probable that prelithification structures such as mixed zones can be preserved through protracted post-lithification deformation, and may in fact form the host rock to these later structures. This has implications for correlating and interpreting the deformational, burial, diagenetic, and fluid-flow histories of faults and their host rocks (cf. Hippler, 1997; Byrne, 1994).

Acknowledgments

This work was supported by the National Science Foundation (grants EAR-9706482 and EAR 9526983), the New Mexico Geological Society, and the New Mexico Department of Safety. We thank Sean Connell for discussions on Albuquerque Basin geology, and Nelia Dunbar and Lynn Heizler for assistance with the microprobe. Comments by Adam Read, Bill Haneberg, Steve Cather and reviewers Kohtaro Ujiie and Paola Vannuchi improved the manuscript.

References

Antonellini, M., Aydin, A., 1994. Effect of faulting on fluid flow in porous sandstones: petrophysical properties. The American Association of Petroleum Geologists Bulletin 78, 355–377.

Antonellini, M.A., Aydin, A., Pollard, D.A., 1994. Microstrucuture of deformation bands in porous sandstones at Arches National Park, Utah. Journal of Structural Geology 16, 941–959.

Atkinson, J.H., Bransby, P.L., 1978. The Mechanics of Soils: An Introduction to Critical State Soil Mechanics. McGraw-Hill, New York.

Aydin, A., 1978. Small faults formed as deformation bands in sandstones. Pure and Applied Geophysics 116, 913–930.

Aydin, A., Eyal, Y., 2002. Anatomy of a normal fault with shale smear: implications for fault seal. American Association of Petroleum Geologists Bulletin 86, 1367–1381.

Aydin, A., Johnson, A.M., 1978. Development of faults as zones of deformation bands and as slip surfaces in sandstone. Pure and Applied Geophysics 116, 931–942.

Beckner, J., Mozley, P.S., 1998. Origin and spatial distribution of early phreatic and vadose calcite cements in the Zia Formation, Albuquerque Basin, New Mexico, USA. In: Morad, S. (Ed.), Carbonate Cements in Sandstones. International Association of Sedimentologists, Special Publication 26, 27–51.

Been, K., Jefferies, M.G., Hachey, J., 1991. The critical state of sands: Geotechnique 41, 365–381.

Bense, V.F., Van den Berg, E.H., Van Balen, R.T., 2003. Deformation mechanisms and hydraulic properties of fault zones in unconsolidated sediments; the Roer Valley Rift System, The Netherlands. Hydrogeology Journal 11, 319–332.

Bishop, A.W., 1975. The strength of soils as engineering materials. In: Milestones in Soil Mechanics: The First Ten Rankine Lectures. Thomas Telford Ltd. for the Institution of Civil Engineers, pp. 91–128.

Bolton, A.J., Maltman, A.J., Clennell, M.B., 1998. The importance of overpressure timing and permeability evolution in fine-grained sediments undergoing shear. Journal of Structural Geology 20, 1013–1022.

Bredehoeft, J.D., Belitz, K., Sharp-Hansen, S., 1992. The hydrodynamics of the Bighorn Basin: a study of the role of faults. American Association of Petroleum Geologists Bulletin 76, 530–546.

Byrne, T., 1994. Sediment deformation, dewatering and diagenesis: illustrations from selected melange zones. In: Maltman, A. (Ed.), The Geological Deformation of Sediments. Chapman and Hall, London, pp. 239–260.

Caine, J.S., Evans, J.P., Forster, C.B., 1996. Fault zone architecture and permeability structure. Geology 24, 1025–1028.

Caine, J.S., Minor, S.A., Grauch, V.J.S., Hudson, M.R., 2002. Potential for fault zone compartmentalization of groundwater aquifers in poorly lithified, Rio Grande rift-related sediments, New Mexico. Abstracts with Programs—Geological Society of America 34, 59.

Cheng, C.H., Johnston, D.H., 1981. Dynamic and static moduli. Geophysical Research Letters 8, 39–42.

Chester, F.M., Chester, J.S., 1998. Ultracataclasite structure and friction processes of the Punchbowl fault, San Andreas system, California. Tectonophysics 295, 199–221.

Chester, F.M., Logan, J.M., 1986. Implications for mechanical properties of brittle faults from observations of the Punchbowl fault zone, California. Pure and Applied Geophysics 124, 79–106.

Chester, F.M., Evans, J.P., Biegel, R.L., 1993. Internal structure and weakening mechanisms of the San Andreas fault. Journal of Geophysical Research 98, 771–786.

Childs, C., Nicol, A., Walsh, J.J., Watterson, J., 1996a. Growth of vertically segmented normal faults. Journal of Structural Geology 18, 1389–1397.

Childs, C., Watterson, J., Walsh, J.J., 1996b. A model for the structure and development of fault zones. Journal of the Geological Society (London) 153, 337–340.

Childs, C., Walsh, J.J., Watterson, J., 1997. Complexity in fault zone structure and implications for fault seal prediction. In: Moller-Pedersen, P., Koestler, A.G. (Eds.), Hydrocarbon Seals: Importance for Exploration and Production. Norwegian Petroleum Society, Special Publication 7. Elsevier, Singapore, pp. 61–72.

Cladouhos, T.T., 1999. Shape preferred orientations of survivor grains in fault gouge. Journal of Structural Geology 21, 419–436.

Connell, S.D., Koning, D.J., Cather, S.M., 1999. Revisions to the stratigraphic nomenclature of the Santa Fe Group, northwestern Albuquerque Basin, New Mexico. In: Pazzaglia, F.J., Lucas, S.G. (Eds.), Albuquerque Geology. New Mexico Geological Society Guidebook, 50, pp. 337–353.

Cowan, D.S., Cladouhos, T.T., Morgan, J.K., 2003. Structural geology and kinematic history of rocks formed along low-angle normal faults, Death Valley, California. Geological Society of America Bulletin 115, 1230–1248.

Doughty, P.T., 2003. Clay smear seals and fault sealing potential of an exhumed growth fault, Rio Grande rift, New Mexico. The American Association of Petroleum Geologists Bulletin 87, 427–444.

Ellen, S.D., Fleming, R.W., 1987. Mobilization of debris flows from soil slips, San Francisco Bay region, California. In: Costa, J.E., Wieczorek, G.F. (Eds.), Mobilization of Debris Flows from Soil Slips, San Francisco Bay Region, California. Geological Society of America Reviews in Engineering Geology, 7, pp. 31–40.

Evans, J.P., Forster, C.B., Goddard, J.V., 1997. Permeability of fault related rocks, and implications for hydraulic structure of fault zones. Journal of Structural Geology 19, 1393–1404.

Foxford, K.A., Walsh, J.J., Watterson, J., Garden, I.R., Guscott, S.C., Burley, S.D., 1998. Structure and content of the Moab Fault Zone, Utah, USA, and its implications for fault seal prediction. In: Jones, G., Fisher, Q.J., Knipe, R.J. (Eds.), Faulting, Fault Sealing, and Fluid Flow in Hydrocarbon Reservoirs. Geological Society of London, Special Publication 147, pp. 87–103.

Goodwin, L.B., Tikoff, B., 2001. Competency contrast, kinematics, and the development of foliations and lineations in the crust. Journal of Structural Geology 24, 1065–1085.

Haneberg, W.C., 1995. Steady-state groundwater flow across idealized faults. Water Resources Research 31, 1815–1820.

Haneberg, W.C., 1999. Effects of valley incision on the subsurface state of stress—theory and application to the Rio Grande valley near Albuquerque, New Mexico. Environmental and Engineering Geoscience 5, 117–131.

Hawley, J.W., Whitworth, T.M., 1996. Hydrogeology of potential recharge areas for the basin- and valley-fill aquifer systems, and hydrogeochemical modeling of proposed artificial recharge of the upper Santa Fe aquifer,

northern Albuquerque Basin: New Mexico Bureau of Mines and Mineral Resources Open-File Report 402 D.

Hawley, J.W., Haase, C.S., Lozinsky, R.P., 1995. The Water Future of Albuquerque and the Middle Rio Grande Basin. In: An underground view of the Albuquerque Basin. New Mexico Water Resources Research Institute Report, 290, pp. 37–55.

Herrin, M., 2001. Characteristics of deformation bands in poorly lithified sand, Rio Grande rift, New Mexico. M.S. Thesis, New Mexico Institute of Mining and Technology.

Heynekamp, M.R., Goodwin, L.B., Mozley, P.S., Haneberg, W.C., 1999. Controls on fault-zone architecture in poorly lithified sediments, Rio Grande Rift, New Mexico: implications for fault-zone permeability and fluid flow. In: Haneberg, W.C., Mozley, P.S., Moore, J.C., Goodwin, L.B. (Eds.), Faults and Subsurface Fluid Flow in the Shallow Crust. American Geophysical Union Geophysical Monograph, 113, pp. 27–49.

Hippler, S.J., 1997. Microstructures and diagenesis in North Sea fault zones: implications for fault-seal potential and fault migration rates. In: Surdam, R.C. (Ed.), Seals, Traps, and the Petroleum System. American Association of Petroleum Geologists Memoir, 67, pp. 85–101.

Jones, M.E., 1994. Mechanical principles of sediment deformation. In: Maltman, A. (Ed.), The Geological Deformation of Sediments. Chapman and Hall, London, pp. 37–71.

Jones, M.E., Addis, M.A., 1984. Volume change during sediment diagenesis and the development of growth faults. Marine and Petroleum Geology 1, 118–122.

Jones, M.E., Addis, M.A., 1986. The application of stress path and critical state analysis to sediment deformation. Journal of Structural Geology 8, 575–580.

Jones, M.E., Preston, R.M.F. (Eds.), 1987. Deformation of Sediments and Sedimentary Rocks. Geological Society of London Special Publication, 29.

Karig, D.E., 1986. Physical properties and mechanical state of accreted sediments in the Nankai Trough, SW Japan. In: Moore, J.C. (Ed.), Structural Fabrics in Deep Sea Drilling Project Cores from Forearcs. Geological Society of America Memoir, 166, pp. 117–133.

Karig, D., Morgan, J., 1994. Tectonic deformation: stress paths and strain histories. In: Maltman, A. (Ed.), The Geological Deformation of Sediments. Chapman and Hall, London, pp. 167–204.

Knipe, R.J., 1993. The influence of fault zone processes and diagenesis on fluid flow. In: Horbury, A.D., Robinson, A.G. (Eds.), Diagenesis and Basin Development. American Association of Petroleum Geologists Studies in Geology, 36, pp. 135–151.

Koning, D.J., 2003. Preliminary Geologic Map of the Chimayo 7.5-minute quadrangle. New Mexico Bureau of Geology and Mineral Resources Open-File Geologic Map OF-GM 71, scale 1, 24000.

Lehner, F.K., Pilaar, W.F., 1997. The emplacement of clay smears in sysnsedimentary normal faults: inferences from field observations near Frechen, Germany. In: Moller-Pedersen, P., Koestler, A.G. (Eds.), Hydrocarbon Seals: Importance for Exploration and Production. Norwegian Petroleum Society, Special Publication 7. Elsevier, Singapore, pp. 39–50.

Lindsay, N.G., Murphy, F.C., Walsh, J.J., Watterson, J., 1993. Outcrop studies of shale smears on fault surfaces. In: Flint, S.S., Bryant, I.D. (Eds.), The Geological Modeling of Hydrocarbon Reservoirs and Outcrop Analogues. International Association of Sedimentologists, Special Publication 15. Blackwell, Oxford, pp. 113–123.

Logan, J.M., Dengo, C.A., Higgs, N.G., Wang, Z.Z., 1992. Fabrics of experimental fault zones: their development and relationship to mechanical behavior. In: Evans, B., Wong, T.-f. (Eds.), Fault Mechanics and Transport Properties of Rocks. International Geophysics Series, 51. Academic Press, London, pp. 33–68.

Mair, K., Main, I., Elphick, S., 2000. Sequential growth of deformation bands in the laboratory. Journal of Structural Geology 22, 25–42.

Menéndez, B., Zhu, W., Wong, T.-f., 1996. Micromechanics of brittle faulting and cataclastic flow in Berea sandstone. Journal of Structural Geology 18, 1–16.

Miller, M.G., 1996. Ductility in fault gouge from a normal fault system, Death Valley, California: a mechanism for fault zone strengthening and relevance to paleoseismicity. Geology 24, 603–606.

Moore, J.C., Byrne, T., 1987. Thickening of fault zones: a mechanism of melange formation in accreting sediments. Geology 15, 1040–1043.

Mozley, P.S., Goodwin, L.B., 1995. Patterns of cementation along a Cenozoic normal fault: a record of paleoflow orientations. Geology 23, 539–542.

Pazzaglia, F.J., Connell, S.D., Hawley, J., Tedford, R.H., Personius, S., Smith, G.A., Cather, S., Lucas, S., Hester, P., Gilmore, J.L.W., 1999. Second-day trip 2 road log, from Albuquerque to San Ysidro, Loma Creston, La Ceja, and Sand Hill fault. In: Pazzaglia, F.J., Lucas, S.G. (Eds.), Albuquerque Geology. New Mexico Geological Society Guidebook, 50, pp. 47–66.

Peacock, D.C.P., Sanderson, D.J., 1992. Effects of layering and anisotropy on fault geometry. Journal of the Geological Society (London) 149, 793–802.

Rawling, G.C., Goodwin, L.B., 2003. Cataclasis and particulate flow in faulted, poorly lithified sediments. Journal of Structural Geology 25, 317–331.

Rawling, G.C., Goodwin, L.B., Wilson, J.L., 2001. Internal architecture, permeability structure, and hydrologic significance of contrasting fault-zone types. Geology 29, 43–46.

Read, A.S., Koning, D.J., Smith, G.A., Ralser, S., Rodgers, J., Bauer, P.W., 2005. Preliminary Geologic Map of the Santa Fe 7.5-minute quadrangle. New Mexico Bureau of Geology and Mineral Resources Open-File Geologic Map OF-GM 32, scale 1, 24000.

Rutter, E.H., 1986. On the nomenclature of mode of failure transitions in rocks. Tectonophysics 122, 381–387.

Rutter, E.H., Maddock, R.H., Hall, S.H., White, S.H., 1986. Comparative microstructures of natural and experimentally produced clay bearing fault gouges. Pure and Applied Geophysics 124, 3–29.

Shelley, D., 1995. Asymmetric shape preferred orientations as shear-sense indicators. Journal of Structural Geology 17, 509–517.

Sigda, J.M., Goodwin, L.B., Mozley, P.S., Wilson, J.L., 1999. Permeability alteration in small-displacement faults in poorly lithified sediments: Rio Grande Rift, Central New Mexico. In: Haneberg, W.C., Mozley, P.S., Moore, J.C., Goodwin, L.B. (Eds.), Faults and Subsurface Fluid Flow in the Shallow Crust. American Geophysical Union Geophysical Monograph, 113, pp. 51–68.

Skempton, A.W., 1985. Residual strength of clays in landslides, folded strata, and in the laboratory. Geotechnique 35, 3–18.

Smith, L., Forster, C., Evans, J., 1990. Interaction of fault zones, fluid flow, and heat transfer at the basin scale. In: Neuman, S.P., Neretnieks, I. (Eds.), Hydrogeology of Low Permeability Environments. Verlag Heinz Heisse, Hannover, Germany, pp. 41–67.

Starkey, J., 1977. The contouring of orientation data represented in spherical projection. Canadian Journal of Earth Sciences 14, 268–277.

Tedford, R.H., Barghoorn, S., 1999. Santa Fe Group (Neogene), Ceja del Rio Puerco, Northwestern Albuquerque Basin, Sandoval County, New Mexico. In: Pazzaglia, F.J., Lucas, S.G. (Eds.), Albuquerque Geology. New Mexico Geological Society Guidebook, 50, pp. 327–335.

Tikoff, B., Wojtal, S.F., 1999. Displacement control of geologic structures. Journal of Structural Geology 21, 959–967.

Ujiie, K., Maltman, A.J., Sanchez-Gomez, M., 2004. Origin of deformation bands in argillaceous sediments at the toe of the Nankai accretionary prism, southwest Japan. Journal of Structural Geology 26, 221–231.

Watterson, J., Childs, C., Walsh, J.J., 1998. Widening of fault zones by erosion of asperities formed by bed-parallel slip. Geology 26, 71–74.

Weber, K.J., Mandl, G., Pilaar, W.F., Lehner, F., Precious, R.G., 1978. The role of faults in hydrocarbon migration and trapping in Nigerian growth fault structures. Proceedings of the Offshore Technology Conference 4, 2643–2653.

Wibberly, C.A.J., Petit, J.-P., Rives, T., 1999. Mechanics of high displacement gradient faulting prior to lithification. Journal of Structural Geology 21, 251–257.

Wong, T.-f., 1990. Mechanical compaction and the brittle-ductile transition in porous sandstones. In: Knipe, R.J., Rutter, E.H. (Eds.), Deformation Mechanisms, Rheology, and Tectonics. Geological Society, Special Publication 54, pp. 111–122.

Wong, T.-f., David, C., Zhu, W., 1997. The transition from brittle faulting to cataclastic flow in porous sandstones: mechanical deformation. Journal of Geophysical Research 102, 3009–3025.